Supplementary Information for:

Epstein-Barr virus BORF2 inhibits cellular APOBEC3B to preserve viral genome integrity

Adam Z. Cheng[1,2,3,4,9], Jaime Yockteng-Melgar[5,9], Matthew C. Jarvis[1,2,3,4], Natasha Malik-Soni[5], Ivan Borozan[6], Michael A. Carpenter[1,2,3,4,8], Jennifer L. McCann[1,2,3,4], Diako Ebrahimi[1,2,3,4], Nadine M. Shaban[1,2,3,4], Edyta Marcon[7], Jack Greenblatt[5,7], William L. Brown[1,2,3,4], Lori Frappier[5] & Reuben S. Harris[1,2,3,4,8]

[1] Department of Biochemistry, Molecular Biology and Biophysics, University of Minnesota, Minneapolis, Minnesota, USA, 55455.
[2] Masonic Cancer Center, University of Minnesota, Minneapolis, Minnesota, USA, 55455.
[3] Institute for Molecular Virology, University of Minnesota, Minneapolis, Minnesota, USA, 55455.
[4] Center for Genome Engineering, University of Minnesota, Minneapolis, Minnesota, USA, 55455.
[5] Department of Molecular Genetics, University of Toronto, Toronto, Ontario, Canada, M5S 1A8.
[6] Ontario Institute for Cancer Research, MaRS Centre, South Tower, 101 College Street, Suite 800, Toronto, Ontario, Canada, M5G 0A3.
[7] Donnelly Centre, University of Toronto, Toronto, Ontario, Canada, M5S 1A8.
[8] Howard Hughes Medical Institute, University of Minnesota, Minneapolis, Minnesota, USA, 55455.
[9] These authors contributed equally to this work.

Table of Contents

Supplementary Figure 1 | AP-MS coverage and A3B expression in human cell lines used in these studies.

a, Amino acid sequence of A3B with residues highlighted in red denoting total peptide coverage from Fig. 1a.

b-d, mRNA expression levels of indicated A3 family members measured by RT-qPCR of (b) 293T, (c) AGS, or (d) AGS-EBV cells, normalized to housekeeping gene *TBP* (mean +/- SD of technical triplicate reactions, N.D., not detectable). These data are representative of n = 2 (c,d) or n = 3 (a,b) biologically independent experiments. RT-qPCR was performed in technical triplicates.

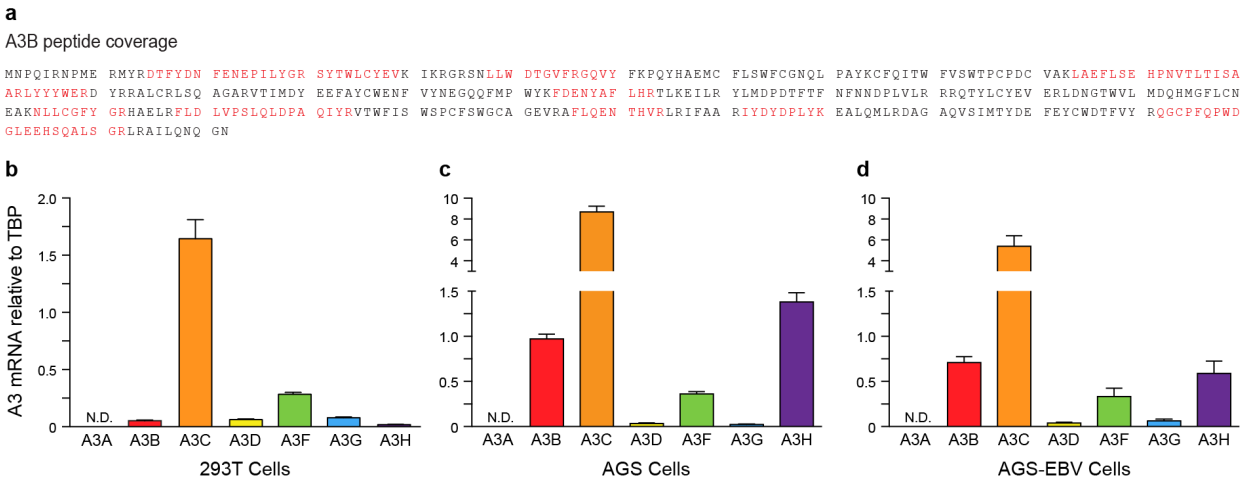

Supplementary Figure 2 | KSHV ORF61 also binds A3B and relocalizes it to perinuclear regions.

a, Co-IP of endogenous A3B in AGS cells with indicated Flag-tagged RNRs. Several RNRs were expressed below detectable levels in whole cell extracts (despite clear detection after IP). Near-equivalent loading of each reaction was indicated by similar levels of endogenous A3B in the whole cell extract input immunoblot.

b-c, Representative fluorescent microscopy images of A3B-eGFP, ORF61-Flag, and the two proteins together in AGS and 293T cells, respectively. A 10 μm scale is shown in the merged panel images. These data are representative of n = 2 (b), n = 3 (c), or n = 4 (a) biologically independent experiments.

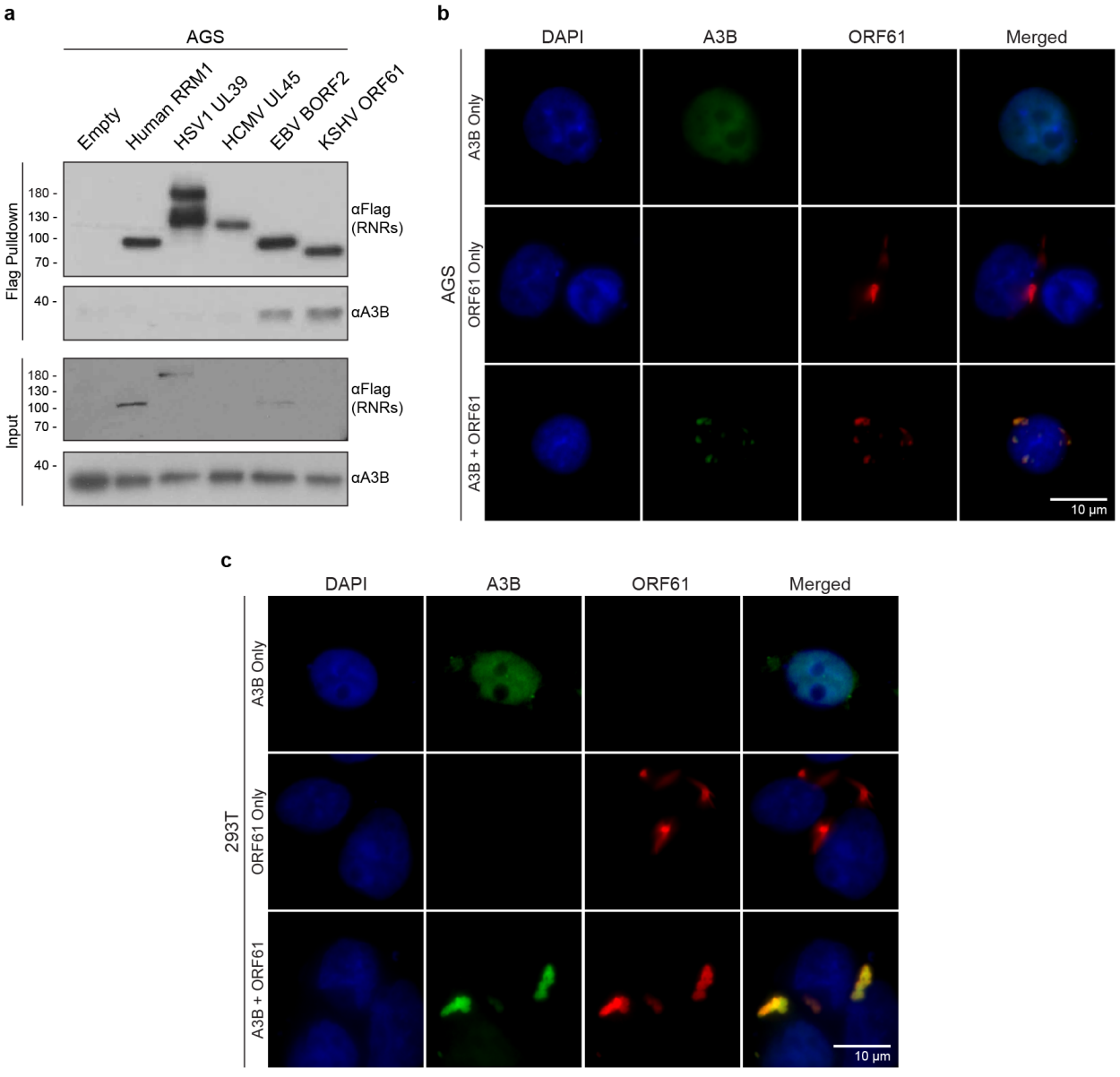

Supplementary Figure 3 | The conserved RNR domain of EBV BORF2 is required for interaction with A3B.

a, Schematics of BORF2 and related RNRs from the indicated herpesviruses.

b, Schematics of BORF2 N- and C-terminal deletion mutants with residue positions indicated.

c, Co-IP results in which the indicated BORF2-Flag N-terminal deletion constructs were pulled-down from 293T cells co-expressing A3B-Strep and/or EBV BaRF1-HA. The BORF2 interaction with A3B requires BORF2 residues 26-50, whereas the interaction with BaRF1 does not.

d, Co-IP results in which the indicated BORF2-Flag C-terminal deletion constructs were pulled-down from 293T cells co-expressing A3B-Strep and/or EBV BaRF1-HA. The BORF2 interaction with A3B requires BORF2 residues 688-739, whereas the interaction with BaRF1 is less dependent on these residues.

e, Co-IP results in which BORF2-Flag and the indicated catalytic mutant derivatives were pulled-down from 293T cells co-expressing human A3B-HA. These data indicated that the catalytic residues of BORF2 are dispensable for interacting with A3B. These data (b-e) are representative of n = 3 biologically independent experiments.

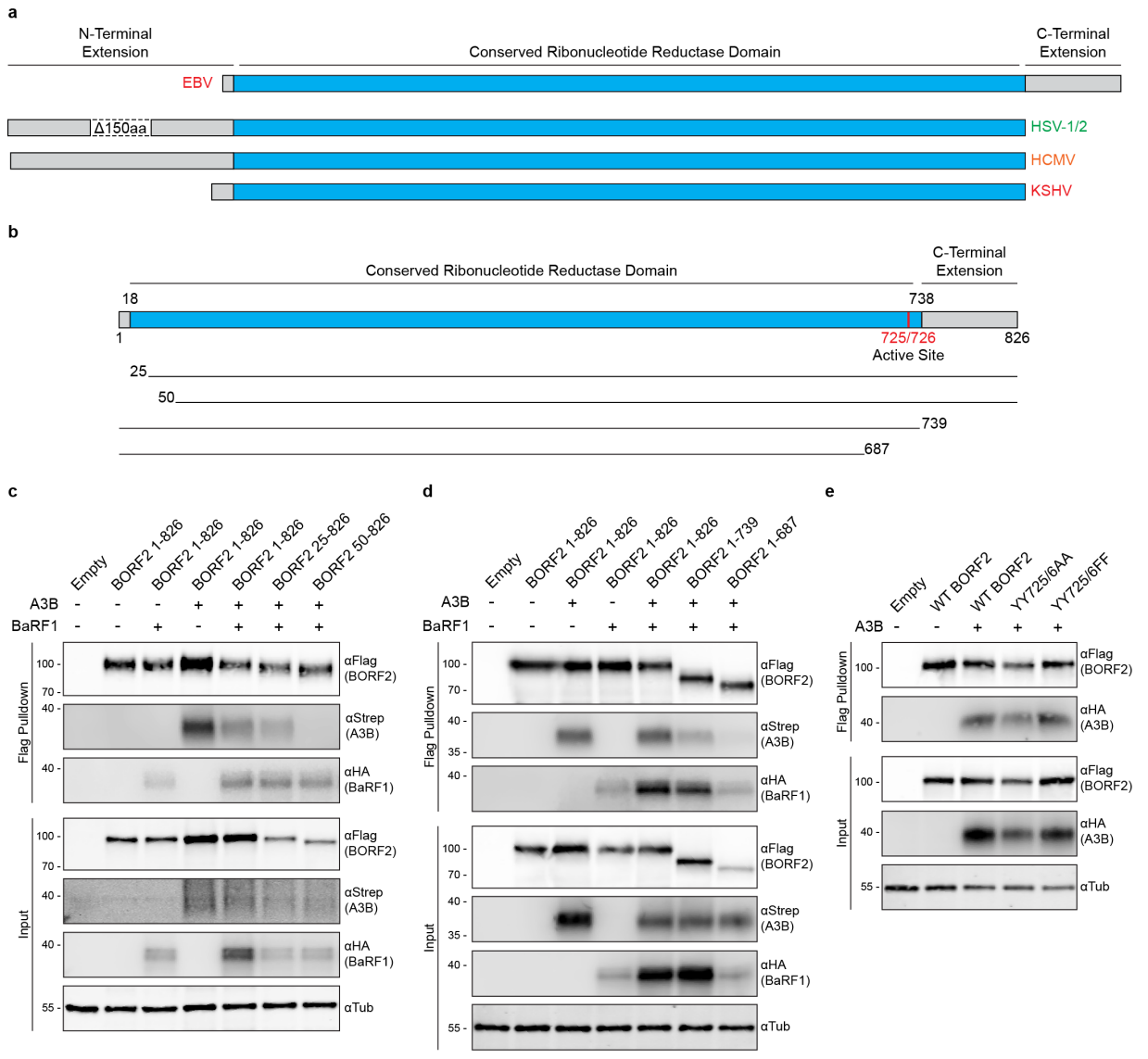

Supplementary Figure 4 | BORF2 does not interact with A3D.
A co-IP experiment using BORF2-Flag to attempt to pull-down A3D-HA from 293T cell lysates. A reconstruction of the experiment in Fig. 1c was necessary for A3D because it is expressed poorly relative to related A3 family members and required higher amounts of transfected DNA to achieve similar expression levels. These data are representative of n = 3 biologically independent experiments.

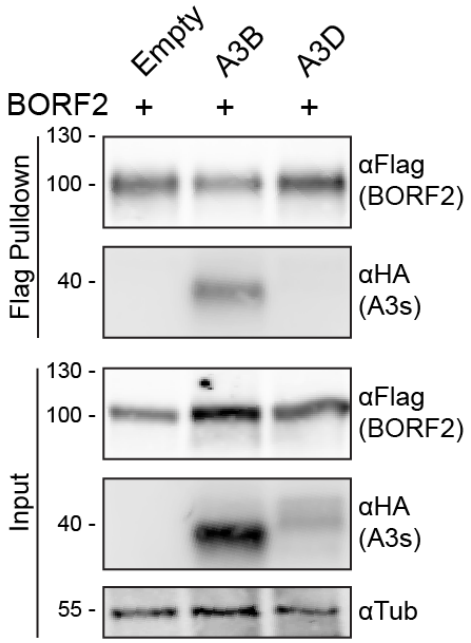

Supplementary Figure 5 | *In vitro* purification of A3H, A3Bctd, and BORF2.
Coomassie stain of SDS-PAGE gel loaded with a BSA standard and aliquots of purified His-SUMO-A3H, His-SUMO-A3Bctd, and His-SUMO-BORF2 from *E. coli*. These proteins were used for deaminase activity assays in Fig. 2. Arrows point to the intact epitope-tagged proteins. As for many EBV proteins, BORF2 was difficult to purify from *E. coli*, but these contaminants do not compromise the conclusions in Fig. 2 where even this relatively crude BORF2 preparation was able to specifically inhibit the activity of A3Bctd but not that of A3H. These data are representative of n = 3 biologically independent experiments.

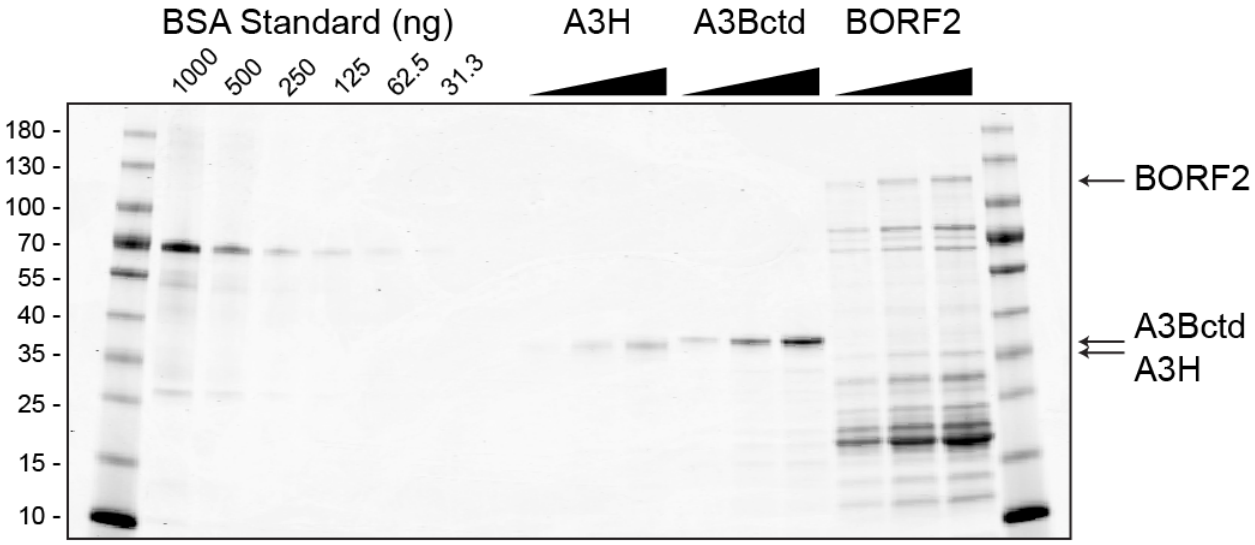

Supplementary Figure 6 | A3B and BORF2 levels are unaffected by MG132 treatment.
a, Immunoblots of whole cell extracts from 293T cells co-transfected with constructs expressing A3B-HA, BORF2-Flag, and/or HIV-1 IIIB Vif-Myc. Cells were transfected and, after 42 hrs, treated for 4 hrs with 10 μM MG132 or vehicle control (DMSO), and harvested for immunoblotting. Neither HIV-1 Vif nor BORF2 caused a significant change in A3B protein levels. **b**, Parallel immunoblot control experiment as in panel (a) except using A3G-HA (instead of A3B-HA). Expression of BORF2-Flag caused a proteasome-independent drop in cellular A3G levels (perhaps due to competition for ribosomes), whereas HIV-1 Vif caused the degradation of A3G through an established proteasome-dependent mechanism (compare band intensities in lanes 2 and 5). These data (a,b) are representative of n = 3 biologically independent experiments.

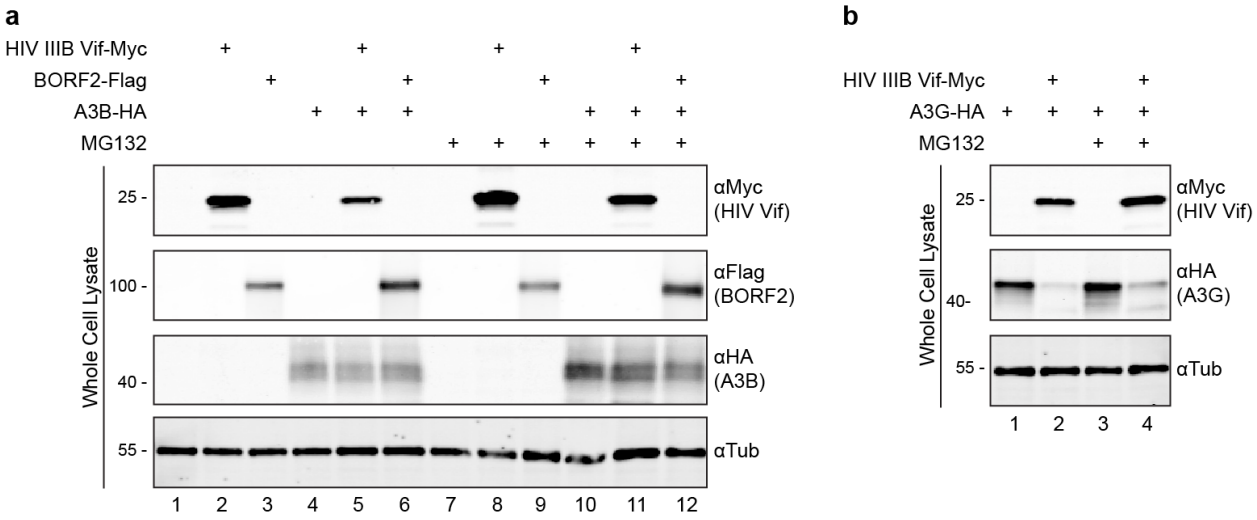

Supplementary Figure 7 | Examples of BORF2 relocalization of A3B in multiple cell types. **a-h**, Representative immunofluorescence microscopy images with the indicated proteins and cell lines. Panels (a-d) show transfected proteins with the indicated C-terminal tags. Panels (e-h) show endogenous proteins stained with antibodies.
i-j, Representative still images from live cell imaging experiments (Extended Data Video 3 & 4, respectively). These data are representative of n = 2 (f-j), n = 3 (a,b,d), or n ≥ 4 (c,e) biologically independent experiments.

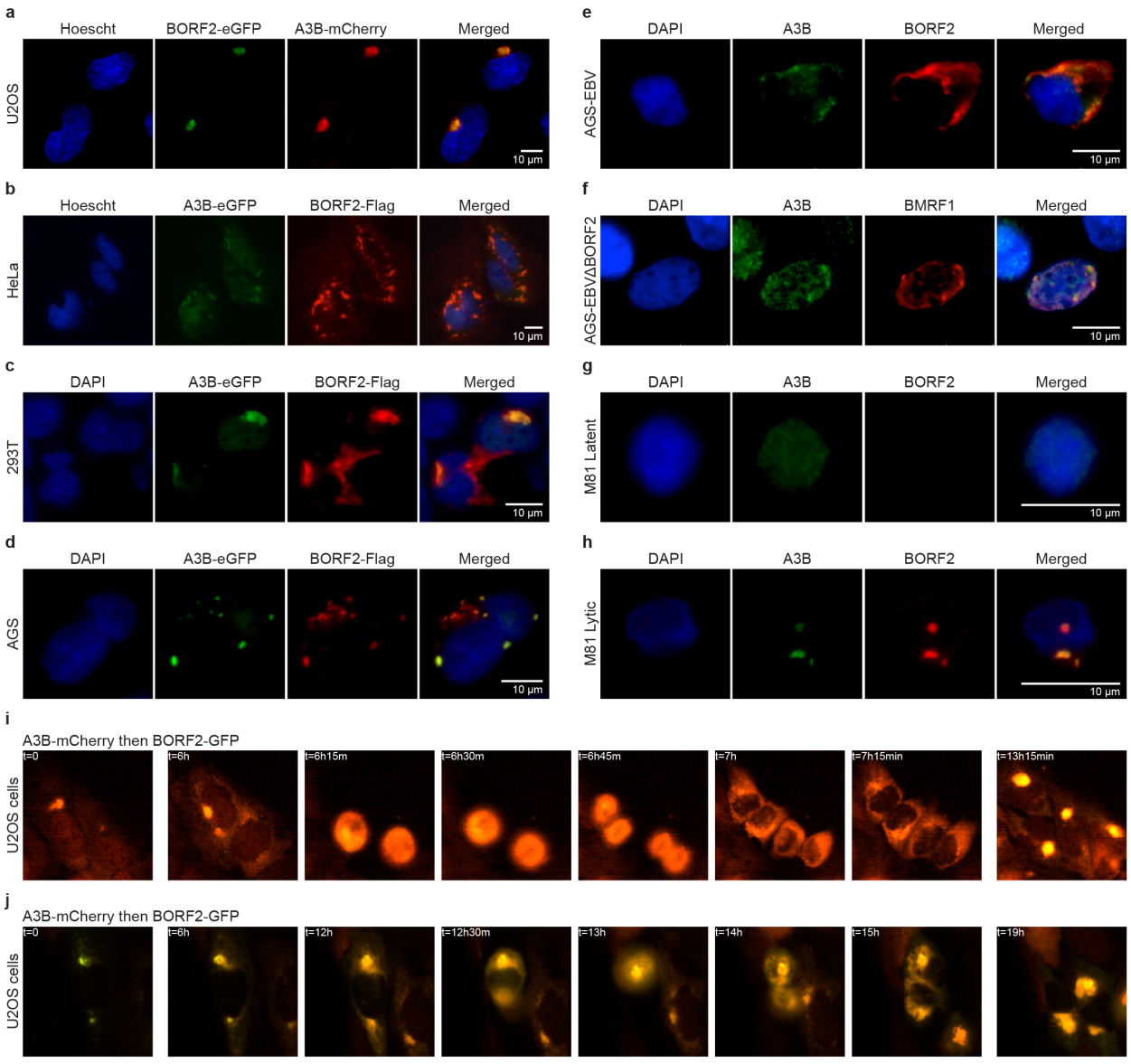

Supplementary Figure 8 | Deletion of BORF2 in EBV episomes in AGS-EBV(Bx1g) and Akata.

a, Schematic of a portion of the BORF2 gene targeted by Cas9 with gRNA complementarity shown in blue, PAM site shown in orange, and predicted endonuclease cut site shown by the red arrow (nucleotide numbers +116 and +139 are relative to BORF2 ATG codon).

b, Sanger sequences of the Cas9/gRNA targeted region of BORF2 PCR cloned from DNA purified from a pool of engineered AGS-EBV(Bx1g) cells. Only mutant sequences were recovered (some multiple times indicated by n), suggesting near complete knockout of BORF2 in the engineered pool.

c, Immunoblots of extracts from parental AGS-EBV(Bx1g) cells and the Cas9/gRNA engineered BORF2-null pool after lytic reactivation. BORF2 protein is undetectable in the engineered pool consistent with the sequencing data in (b). These data (**c**) are representative of n = 3 biologically independent experiments.

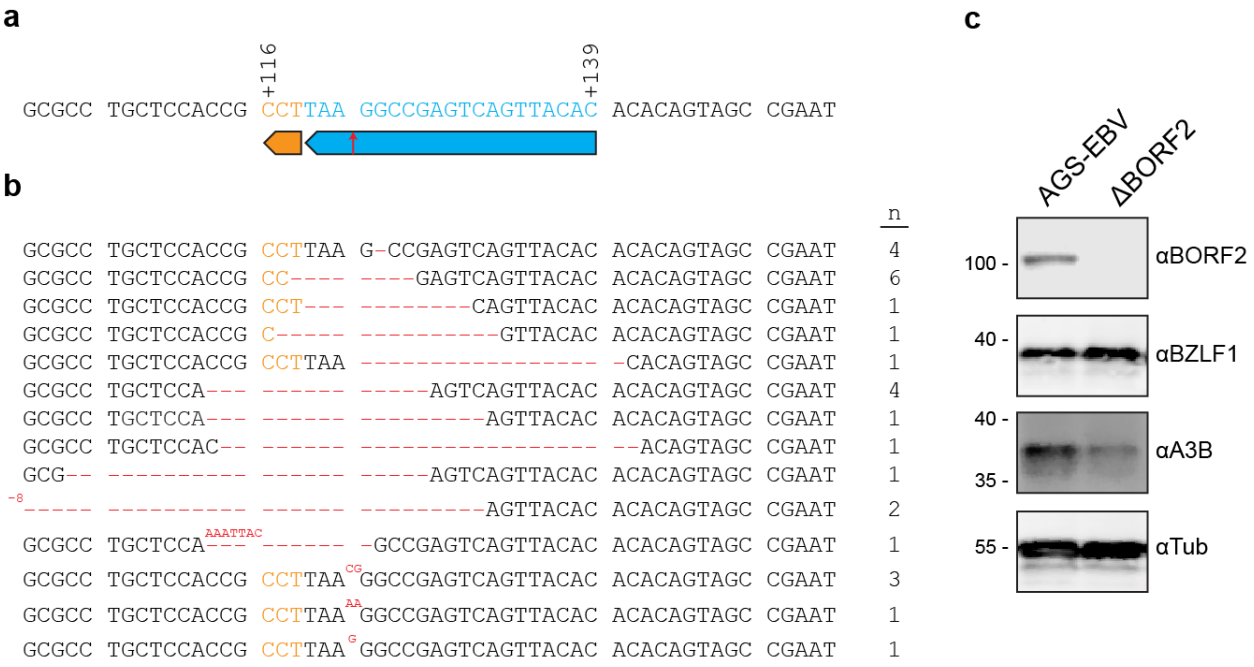

Supplementary Figure 9 | BORF2 functions to preserve EBV genome integrity from A3B.
a, Representative images of agarose gels showing 3D-PCR results of the 254 bp BRRF2 gene segment from pooled BORF2-null AGS-EBV(Bx1g) cells (Supplementary Fig. 7).
b, Pie charts showing number of mutations observed in Sanger sequences of cloned lower temperature amplicons from (a). Wild-type non-mutated sequences depicted in gray and base substitutions shown in orange and red.
c, Agarose gel images of 3D-PCR results using the 217 bp EBNA2 gene segment of derivatives of the AGS-EBV(Bx1g)ΔBORF2 clone. The 16 different conditions labeled below are described in the main text. The faster mobility, low-temperature products from conditions of induced cells, ΔBORF2, shControl, and UGI represent an accumulation of deletion mutations. These data (a,c) are representative of n = 3 biologically independent experiments.

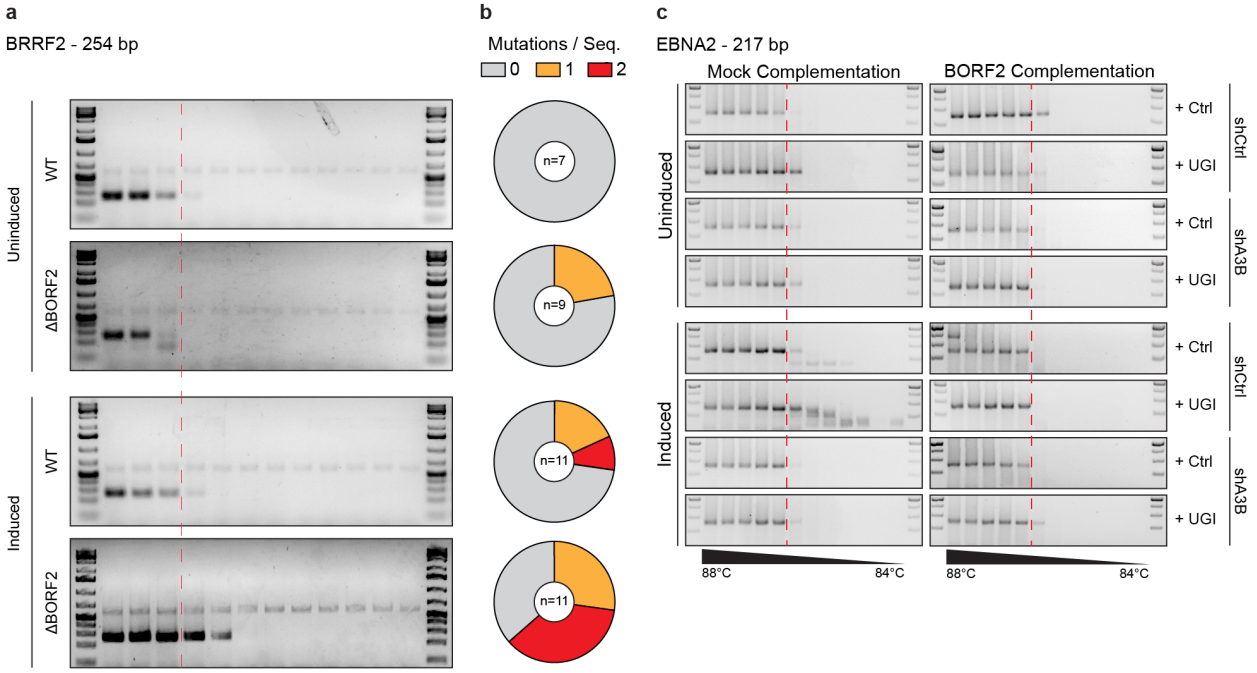

Supplementary Figure 10 | UGI inhibits both cellular UNG2 and EBV uracil DNA glycosylase BKRF3.

a, Schematic of the uracil excision assay.

b, Immunoblot of whole cell lysates from AGS or AGSΔUNG2 cells.

c, Uracil excision experiment in which AGS or AGSΔUNG2 cells were transfected with a construct expressing viral uracil DNA glycosylase (BKRF3) and whole cell lysates were harvested after 30 hrs to test for uracil excision activity in the absence or presence of UGI (see methods for additional information). The uracil excision activity in AGS cells is mostly from cellular UNG2 and inhibited by UGI (compare product bands in lanes 3 vs 7 and 3 vs 4, respectively). BKRF3 expression causes a large increase in uracil excision activity that is almost completely inhibited by UGI (compare lanes 5 vs 6, and lanes 9 vs 10). Negative and positive controls are no UDG and exogenous *E. coli* UDG, respectively. These data are representative of n = 2 (b) or n = 3 (c) biologically independent experiments.

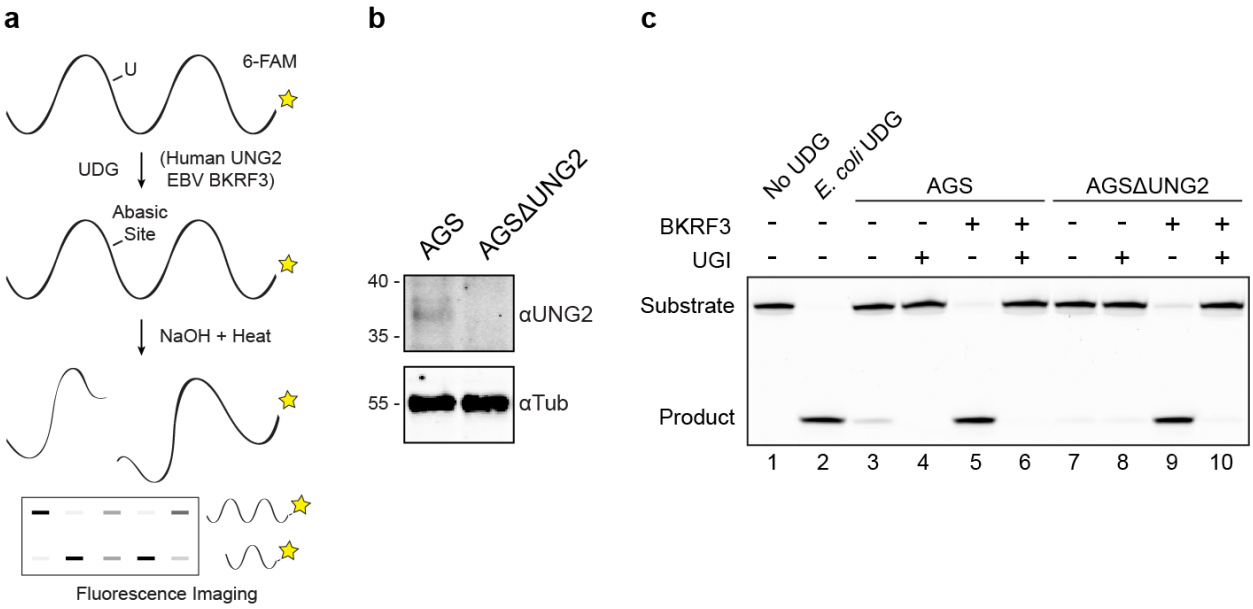

Supplementary Figure 11 | Additional mutation data.
a, Pie charts showing mutational events observed in Sanger sequences of cloned lower temperature 3D-PCR BRRF2 amplicons from the 8 uninduced conditions shown in Fig. 4c (top half). Wild-type non-mutated sequences are depicted in green; base substitutions with numbers of mutations per sequence depicted in light green, yellow, orange, and red; deletions are depicted in black; other types of mutations (*e.g.*, combination of base substitution and deletion) are depicted in navy.
b, Pie charts showing mutational events observed in Sanger sequences of cloned highest temperature BRRF2 amplicons from the 8 induced conditions shown in Fig. 4c (bottom half). Color scheme as in panel (a). A low frequency of hypermutation is expected because lytic reactivation is inefficient (minority of cells in each culture), and EBV lytic replication occurs by coordinated leading- and lagging-strand DNA replication, which is not likely to leave single-stranded DNA exposed for long durations.

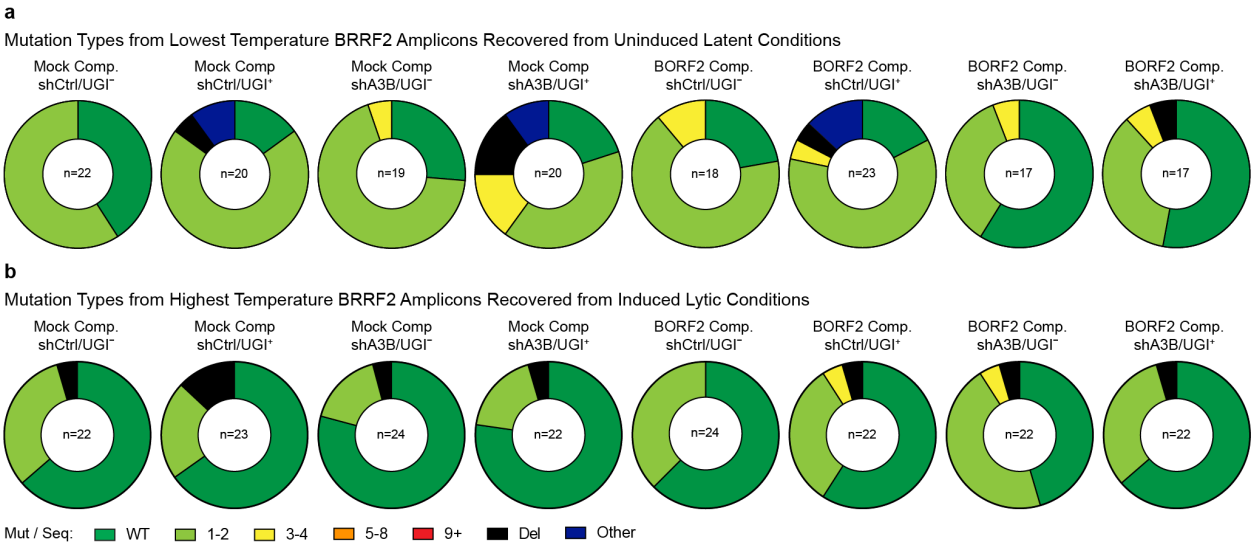

Supplementary Figure 12 | Sanger sequences show massive A3B-dependent hypermutation of EBV lacking BORF2.

Sanger sequences of cloned lower temperature BRRF2 3D-PCR amplicons from the 16 different experimental conditions shown in Fig. 4c. The parental wild-type (WT) BRRF2 sequence is shown in blue (spanning nucleotides +1423 to +1629 relative to the BRRF2 start codon). The pink highlighting shows base substitution mutations and deletion mutations (dashes) within the consensus region. The number of times each sequence was recovered is shown to the right.

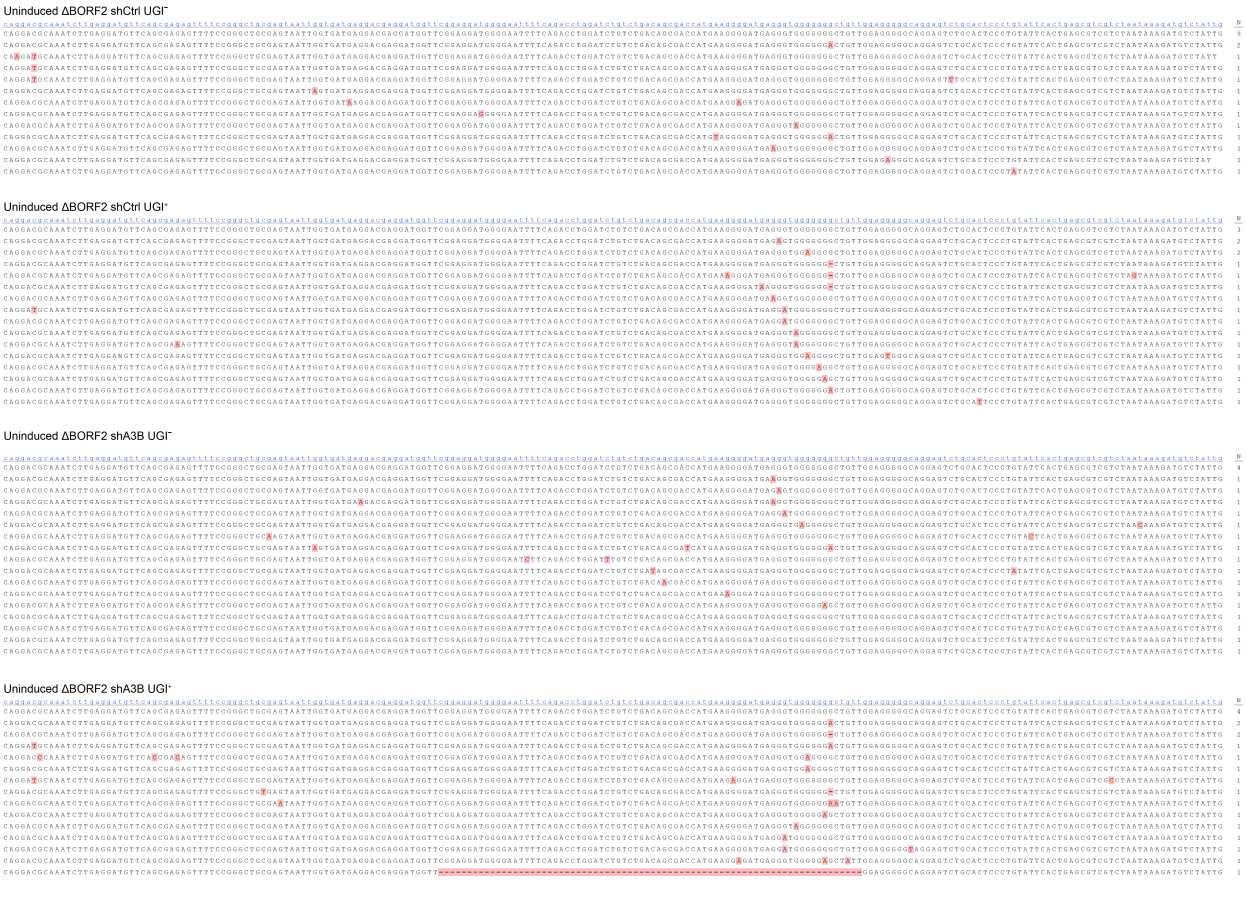

Induced ΔBORF2 shCtrl UGI⁻

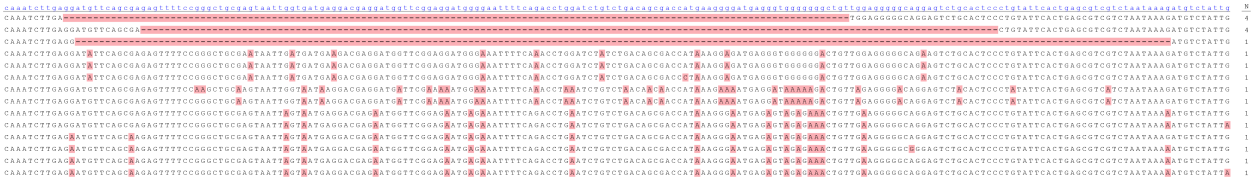

Induced ΔBORF2 shCtrl UGI⁺

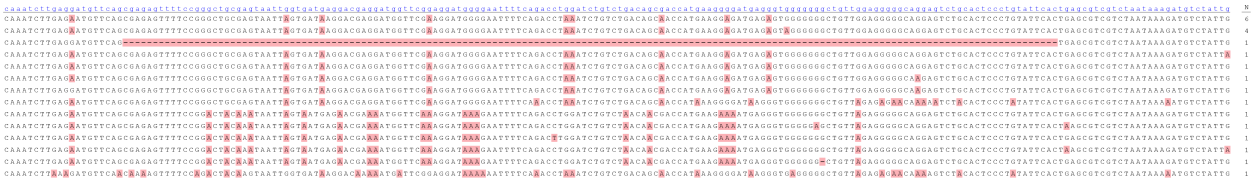

Induced ΔBORF2 shA3B UGI⁻

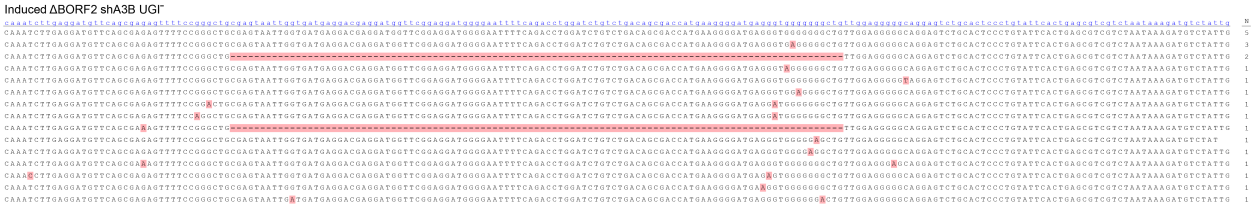

Induced ΔBORF2 shA3B UGI⁺

Induced ΔBORF2 +BORF2 shCtrl UGI⁻

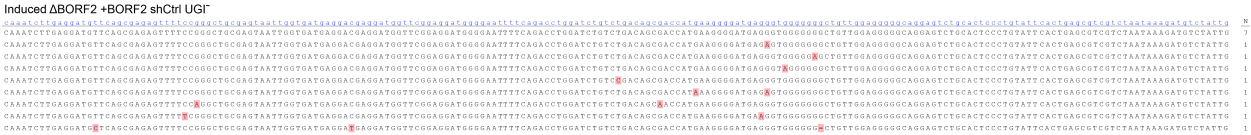

Induced ΔBORF2 +BORF2 shCtrl UGI⁺

Induced ΔBORF2 +BORF2 shA3B UGI⁻

Induced ΔBORF2 +BORF2 shA3B UGI⁺

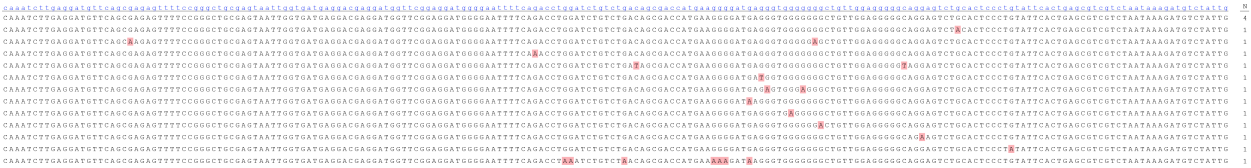

Uninduced ΔBORF2 +BORF2 shCtrl UGI⁻

Uninduced ΔBORF2 +BORF2 shCtrl UGI⁺

Uninduced ΔBORF2 +BORF2 shA3B UGI⁻

Uninduced ΔBORF2 +BORF2 shA3B UGI⁺

Supplementary Figure 13 | BORF2 is dispensable for Akata EBV infectivity.
a, Immunoblots of extracts from parental Akata cells and the Cas9/gRNA engineered BORF2-null pools after lytic reactivation. Endogenous A3B is undetectable in Akata cells (blank immunoblot not shown).
b, Schematic of the A3A and A3B genes (top) and a naturally occurring 29.5 kbp deletion leading an A3A/B fusion gene (bottom, not to scale). Arrows correspond to primer sets used to genotype cells (blue represents the intact locus; red represents the deletion variant).
c, Agarose gel of A3A/B- and A3B-specific PCR products from SKBR3 (A3B-null), MDA-MB-468 (A3B intact), and Akata cells (A3B-null).
d, Infectivity of wild-type and ΔBORF2 viruses produced by lytic replication in Akata cells. Each symbol represents the percent of GFP-positive Ramos reporter cells from n = 3 independent infections, and the horizontal line shows the mean. These data (a,c,d) are representative of n = 3 biologically independent experiments.

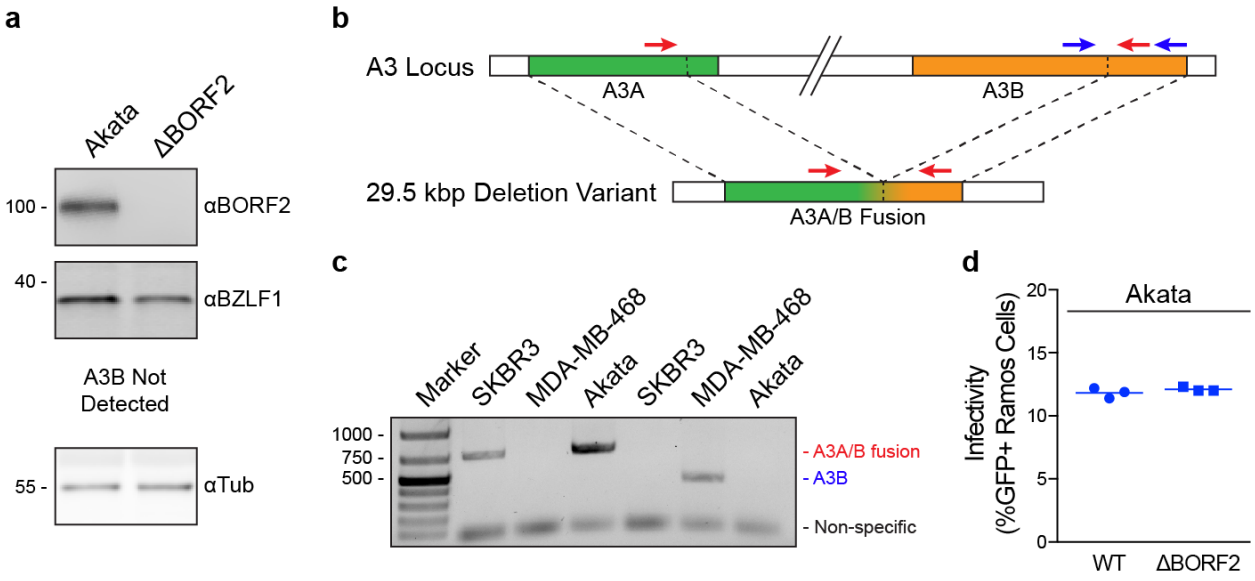

Supplementary Figure 14 | EBV genomic variation in clinical isolates.
a, Bar plot of average ratios of non-synonymous (dN) to synonymous (dS) mutations in every EBV gene centered around 1 (dN = dS) using sequencing data from 142 publically available EBV genomes. Red bars show genes under positive selection while blue bars show genes under negative selection. BORF2 is under strong negative selection consistent with at least one essential function.
b, Schematic of BORF2 gene highlighted with non-synonymous (red triangles) and synonymous (blue triangles) mutations using data from (a). The clustering of amino acid altering base substitutions to the N- and C-terminal ends of BORF2 indicates these regions are dispensable, whereas the majority of the central conserved RNR domain predominantly harbors silent mutations [consistent with result in panel (a) and deletion analysis in Supplementary Fig. 3].
c, Tabulated positions, mutations, and frequencies of every non-synonymous mutation in BORF2.
d, Global distribution of EBV base substitution from 142 clinical EBV isolates showing preferential accumulation of C/G-to-T/A mutations.
e, 1 kbp sliding window analyses in 15 kbp bins of the observed/expected distributions of A3B-preferred 5'-TCA substrates (5'-TGA on complementary strand) and of the most likely transition mutation products 5'-TTA (5'-TAA) within the indicated viral genomes. A3B-preferred deamination substrates are depleted and products are enriched in human EBV and rhesus LCV, but not in murine MHV68 (*i.e.*, A3B, if present, impacts viral trinucleotide distributions). Non-preferred motifs such as 5'-ACA (5'-TGT) are neither depleted nor enriched (data not shown).

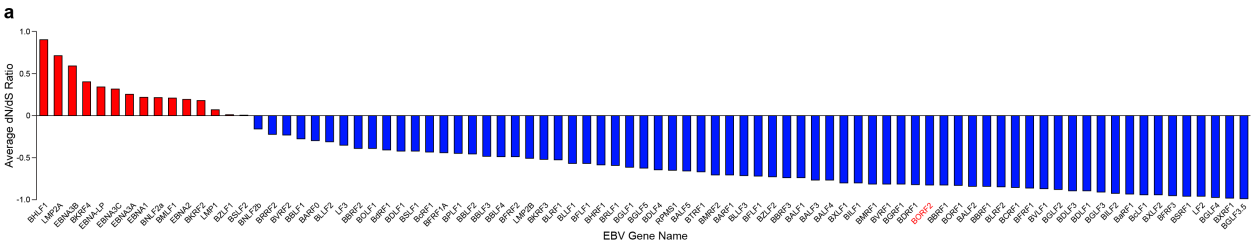

c

Position	Mutation	AA Change	# of Genomes with Mutation	Position	Mutation	AA Change	# of Genomes with Mutation
14	G>A	S5N	53	2051	C>T	A684V	1
17	A>G	H6R	2	2078	A>C	H693P	1
73	T>G	S25A	33	2195	G>A	A733T	1
148	G>A	A50T	11	2240	C>T	S747L	7
250	C>A	P84T	1	2249	G>A	R750Q	1
257	A>T	Y86F	1	2266	C>T	R756W	2
658	G>A	V220I	1	2269	A>G	S757G	2
1244	T>C	V415A	1	2275	G>A	A759T	1
1348	G>A	V450I	11	2288	C>T	P763L	28
1528	C>T	P510S	1	2315	G>A	A773T	15
1530	C>A	P511H	1	2362	G>A	G788S	1
1540	T>A	S514T	2	2407	C>T	R803C	2
1699	A>G	I567V	1				

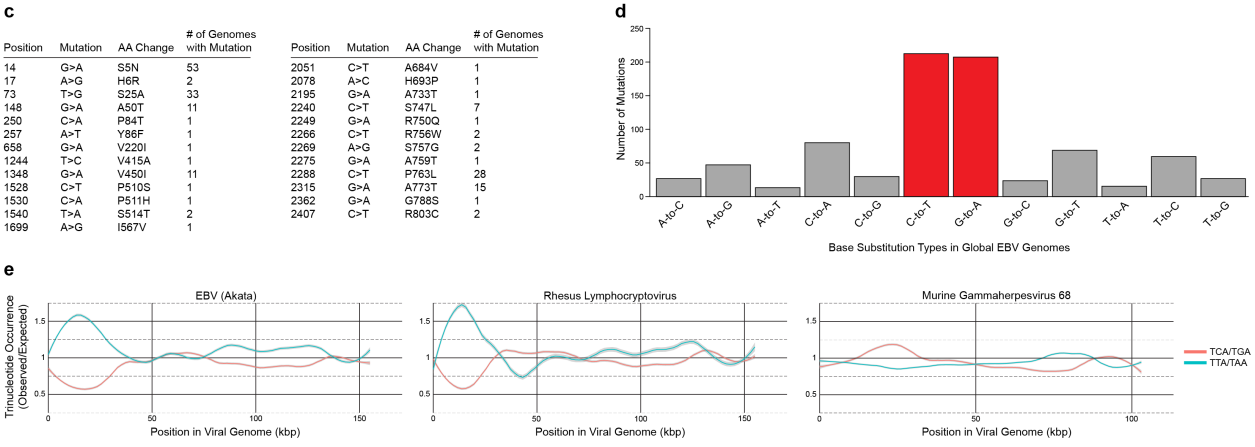

Raw Images for Figure 1

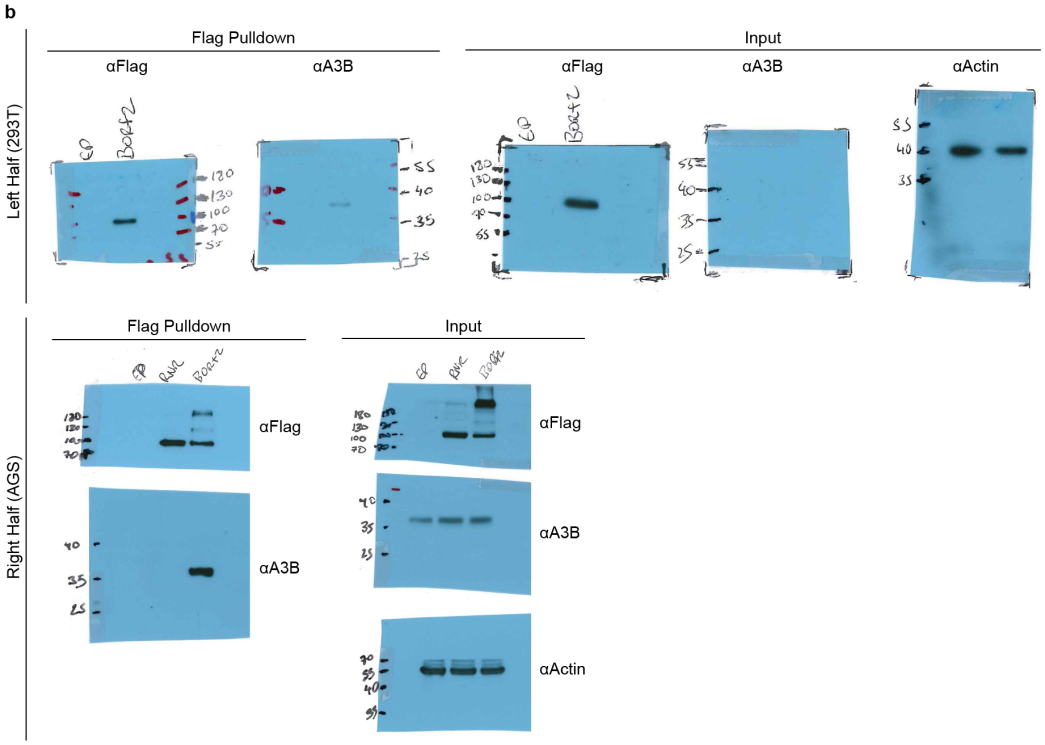

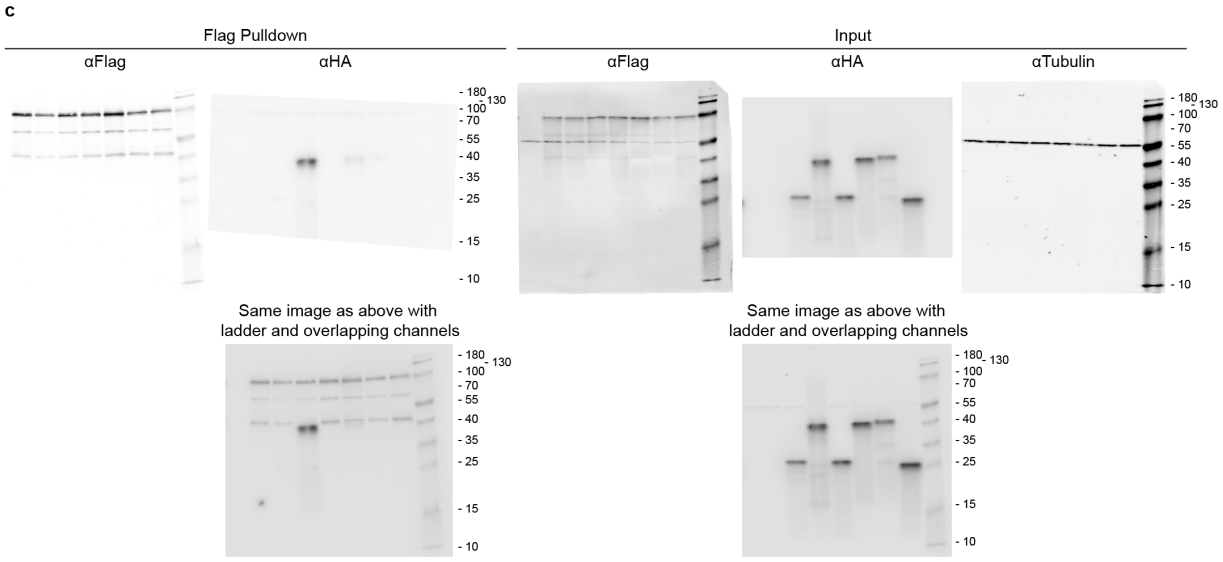

Raw Images for Figure 1 (continued)

d

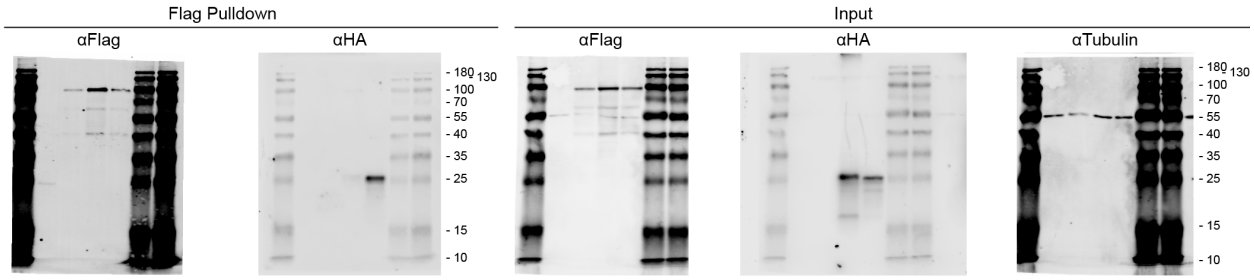

e

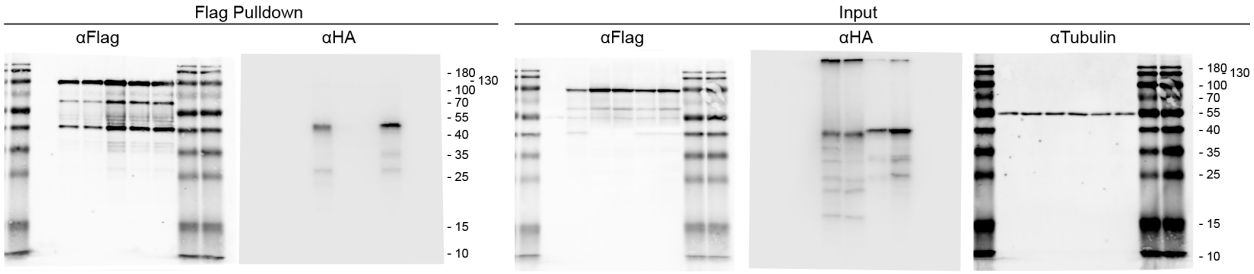

Same image as above with ladder and overlapping channels

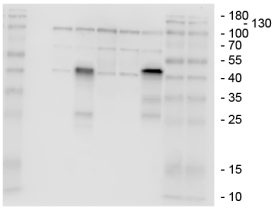

Same image as above with ladder and overlapping channels

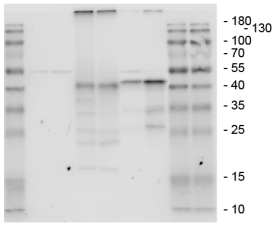

f

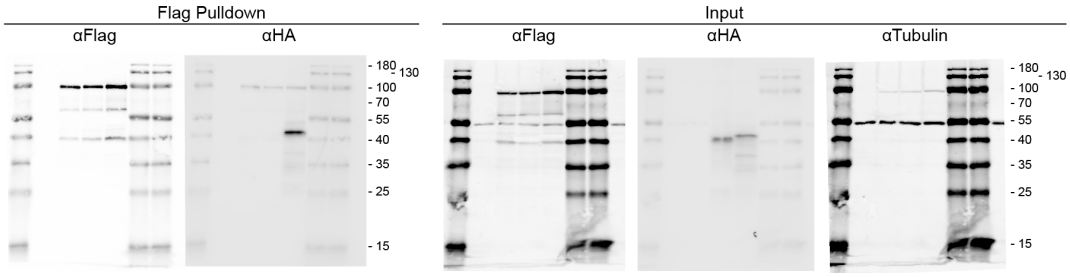

Raw Images for Figure 2

b

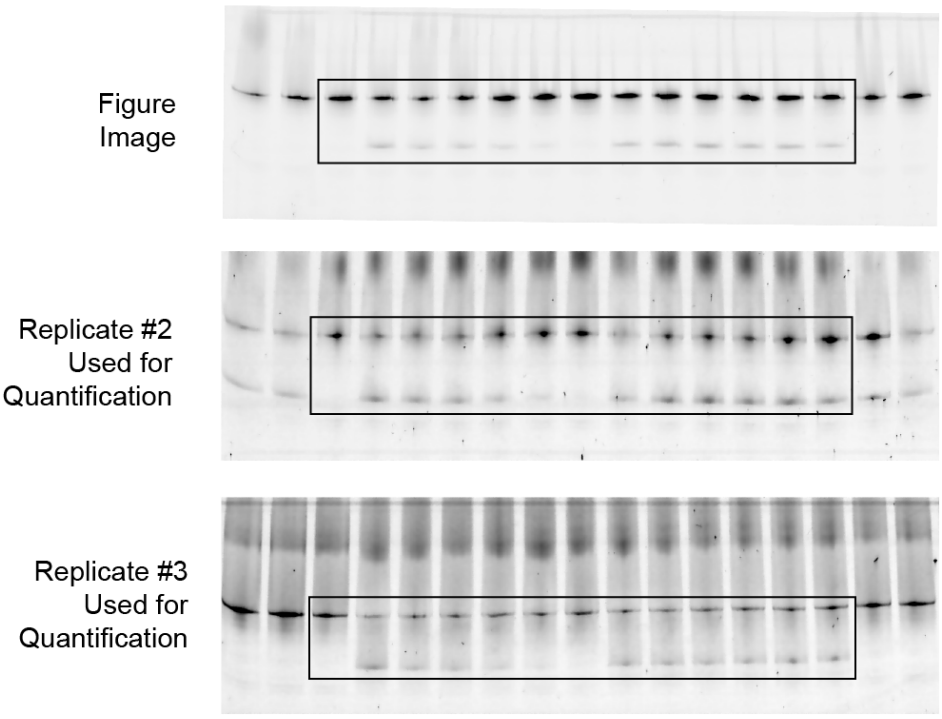

Raw Images for Figure 3

a

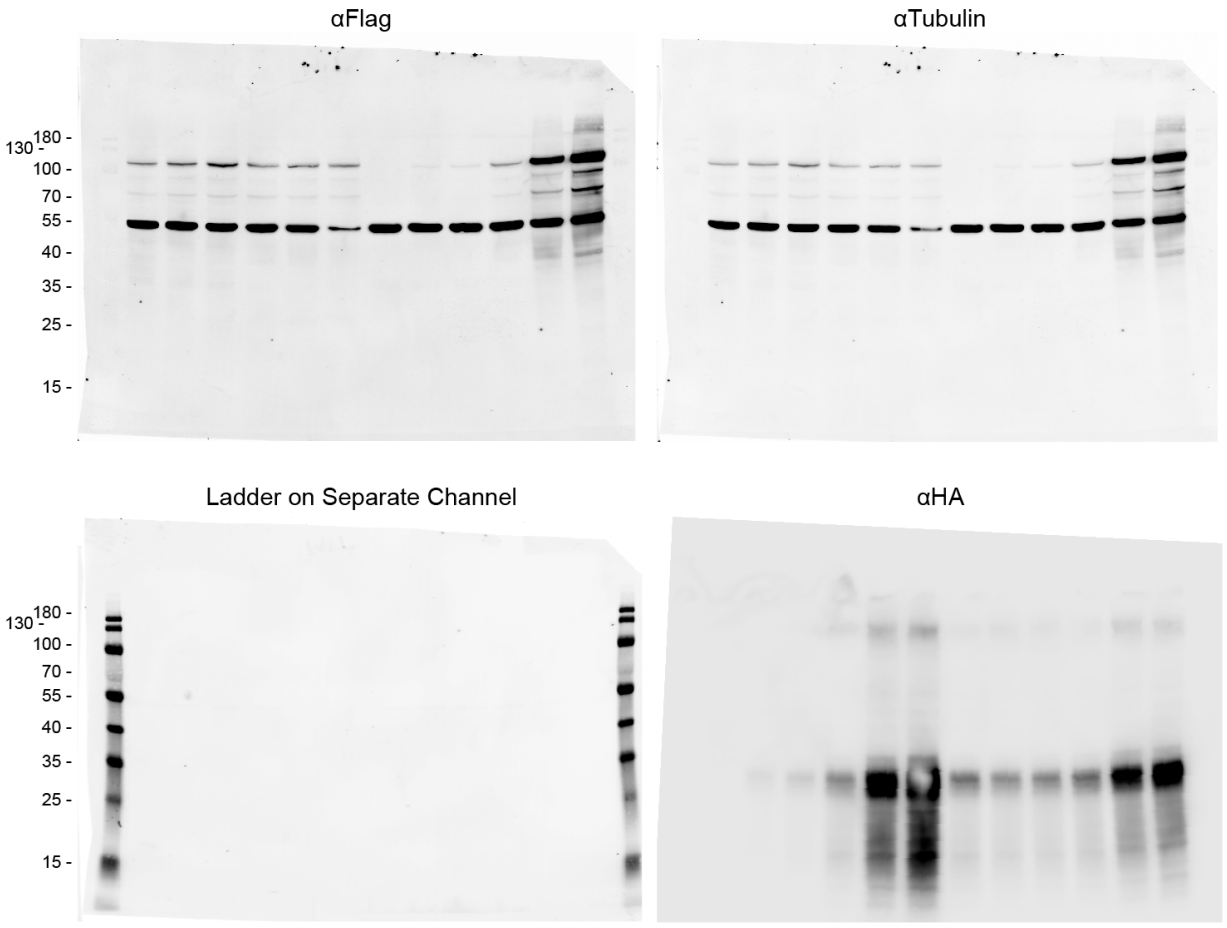

Raw Images for Figure 4

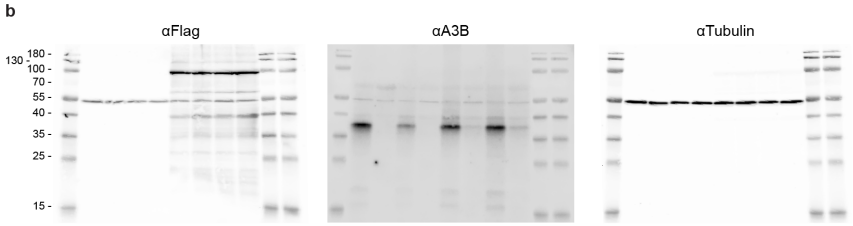

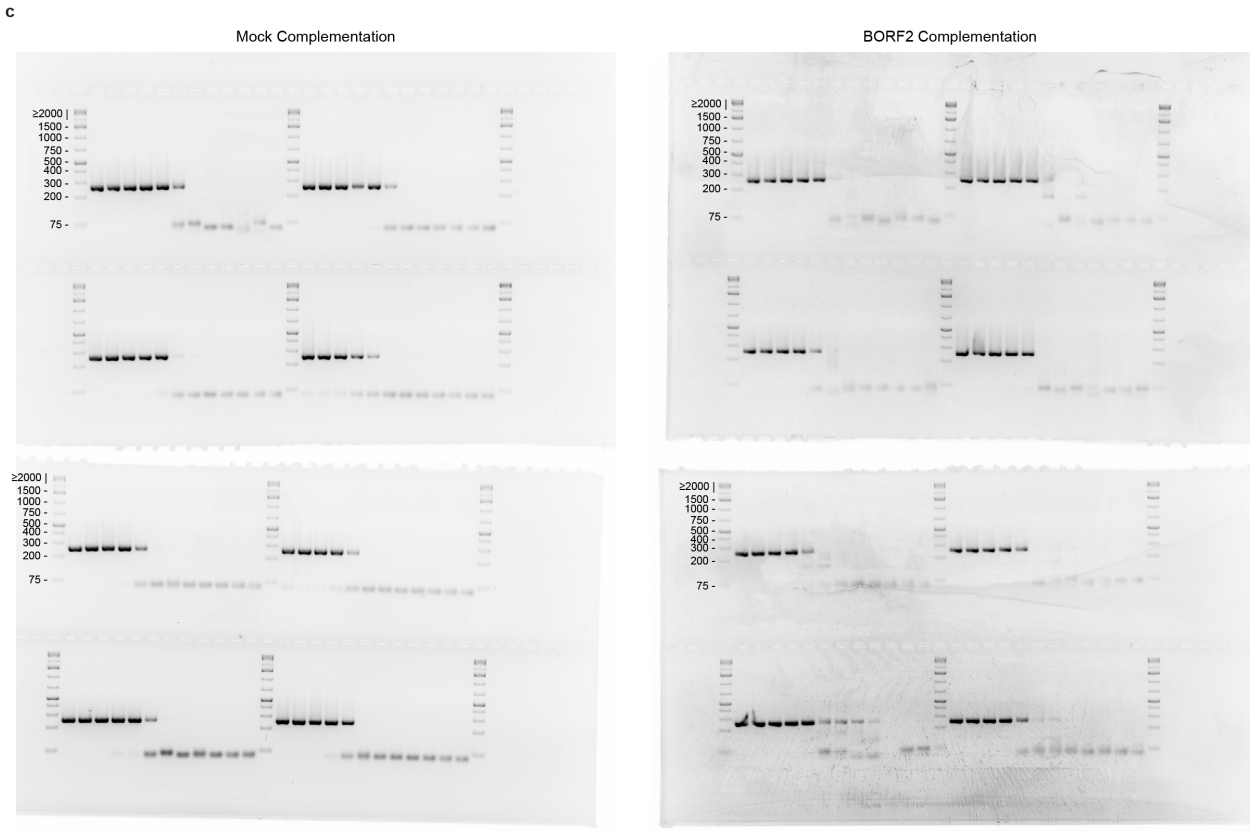

Raw Images for Supplementary Figure 2

a

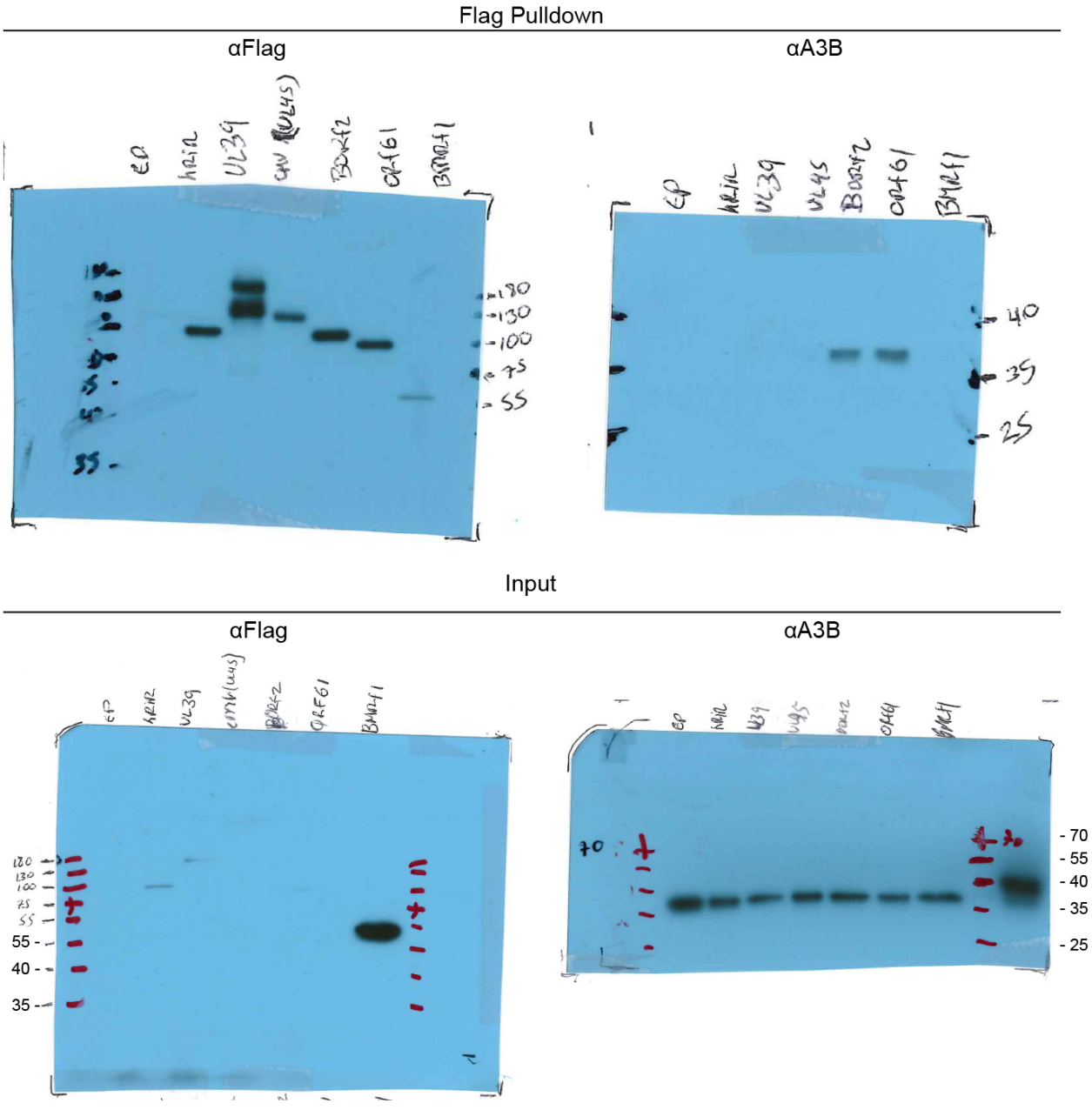

Raw Images for Supplementary Figure 3

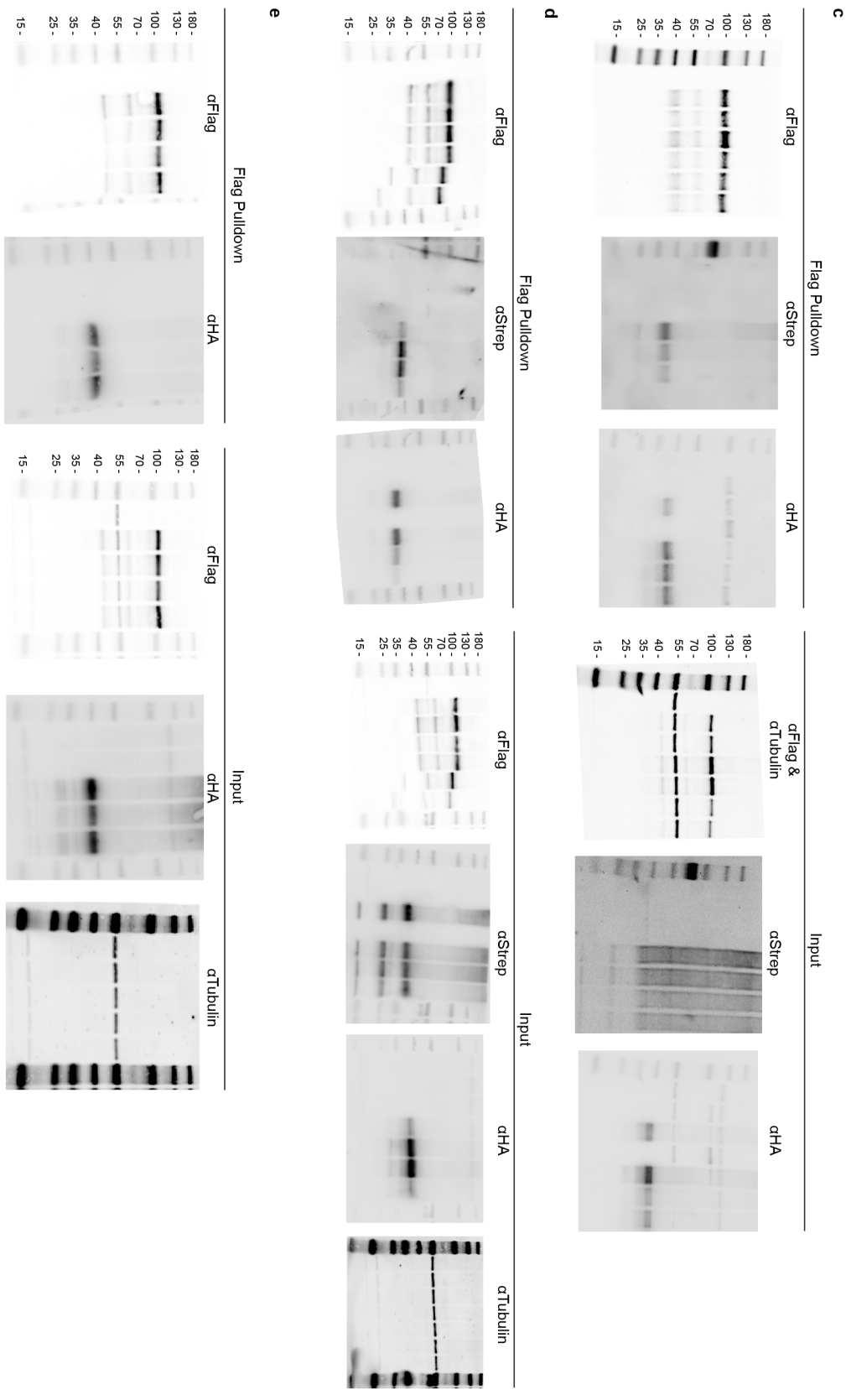

Raw Images for Supplementary Figure 4

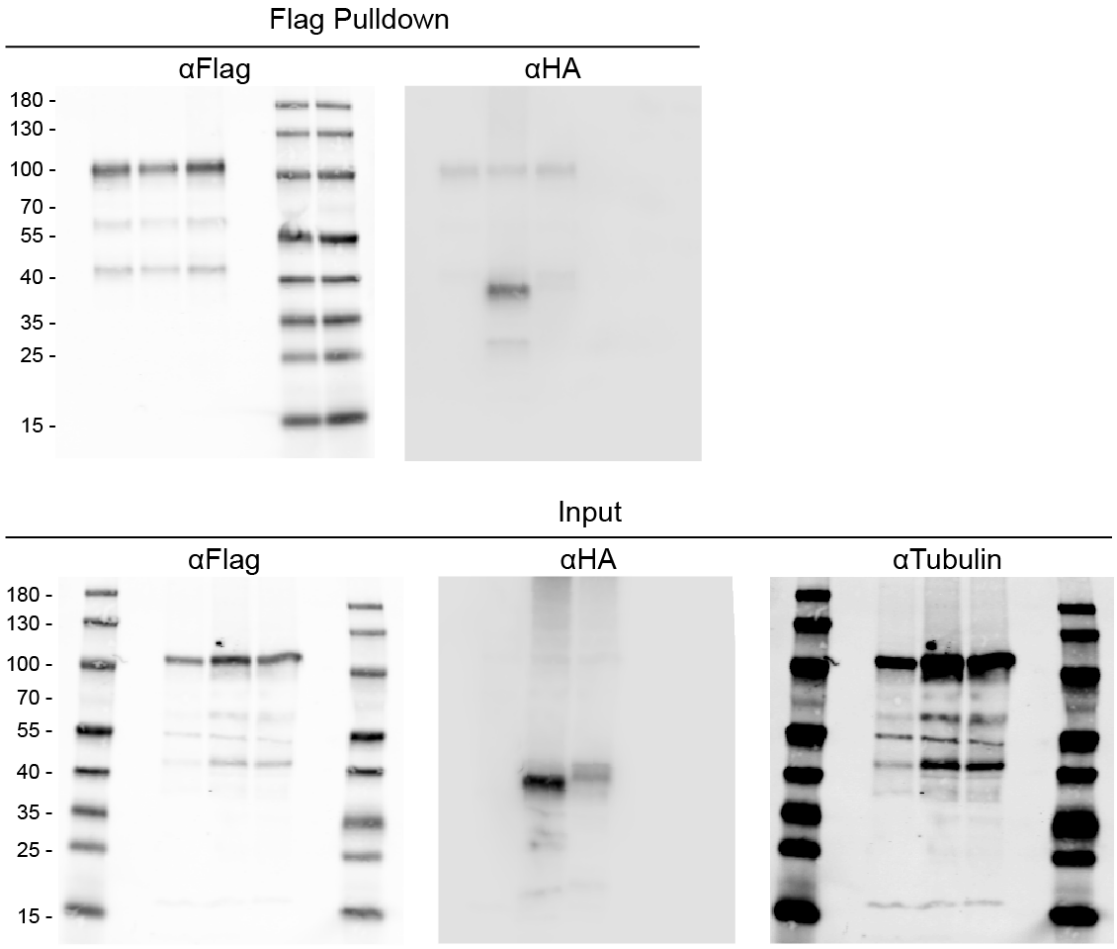

Raw Images for Supplementary Figure 6

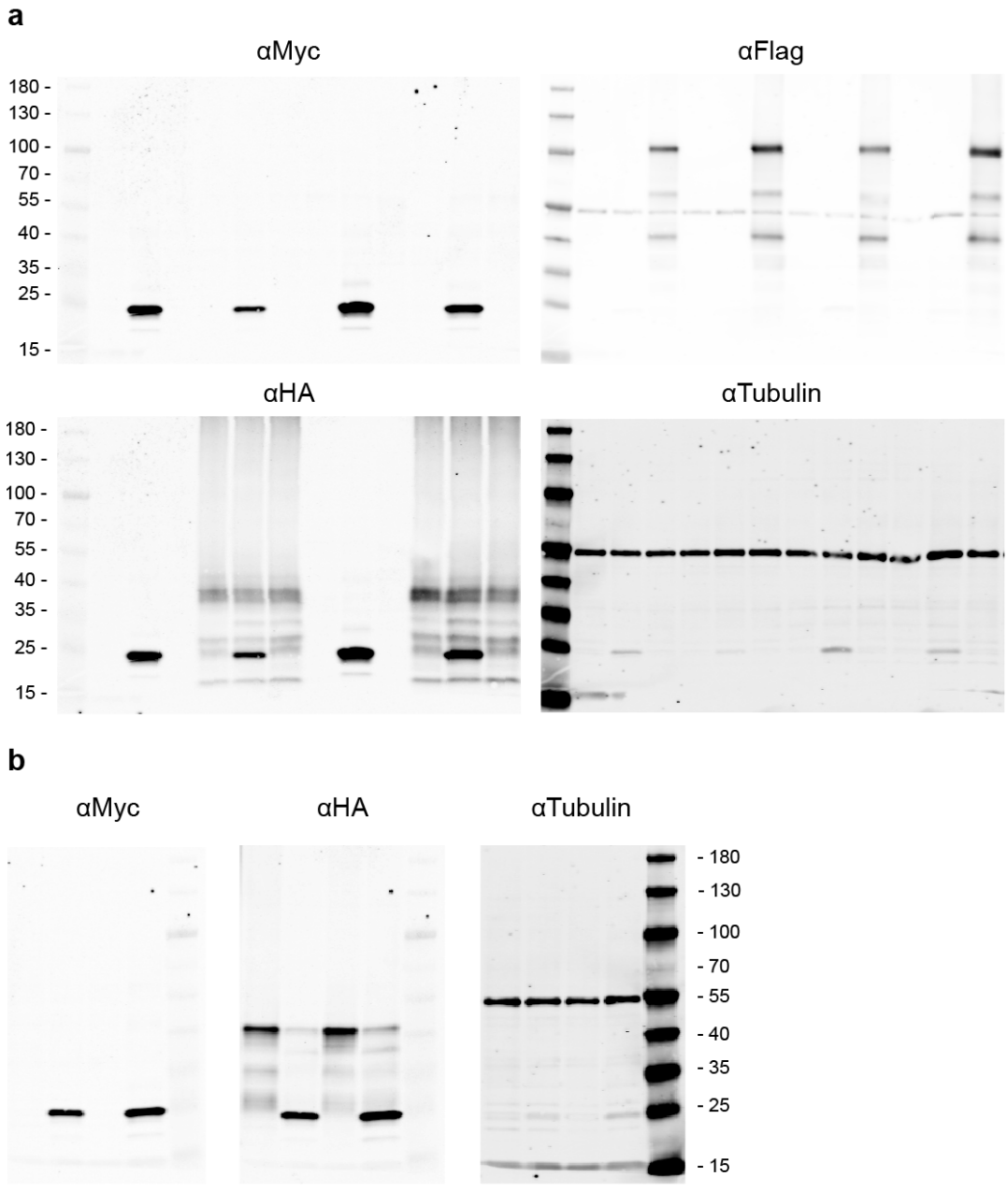

Raw Images for Supplementary Figure 8

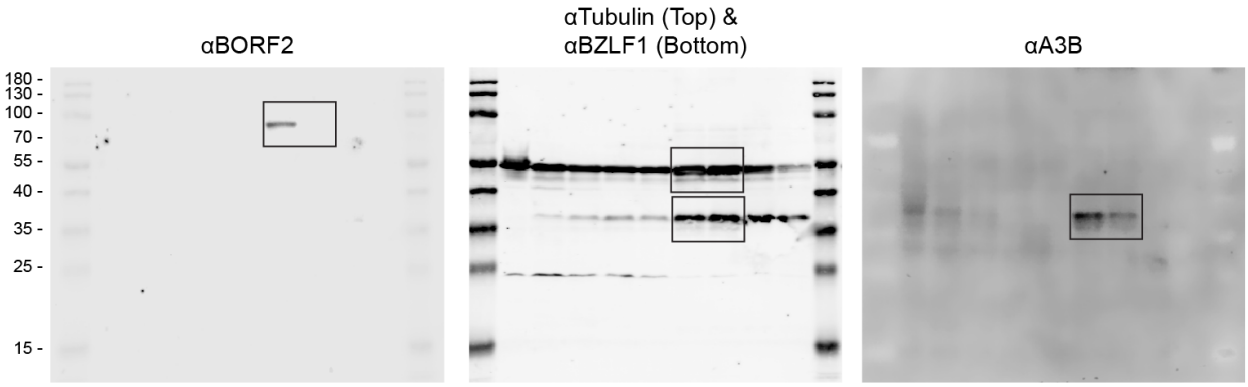

Raw Images for Supplementary Figure 9

Raw Images for Supplementary Figure 10

b

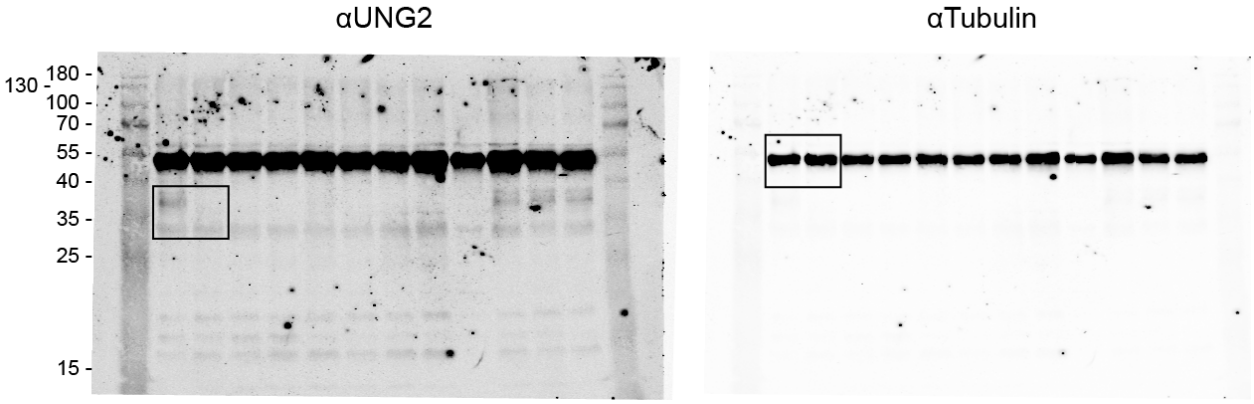

c

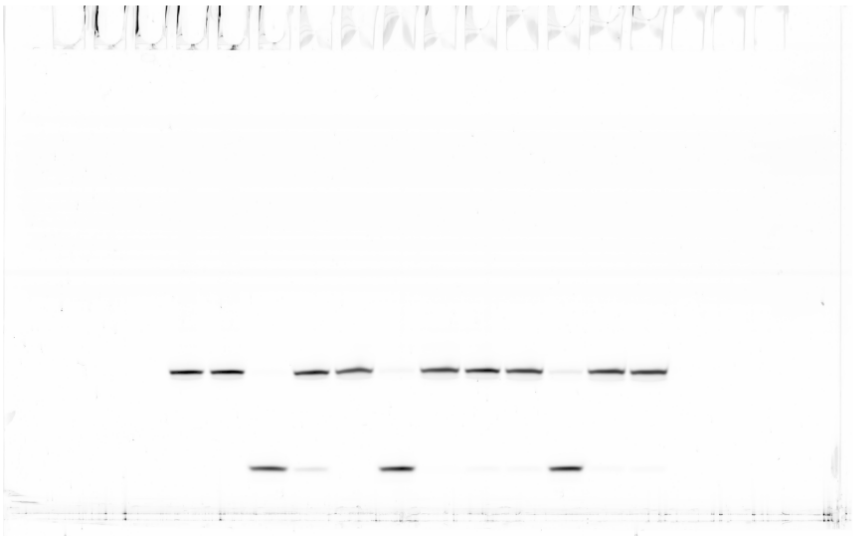

Raw Images for Supplementary Figure 13

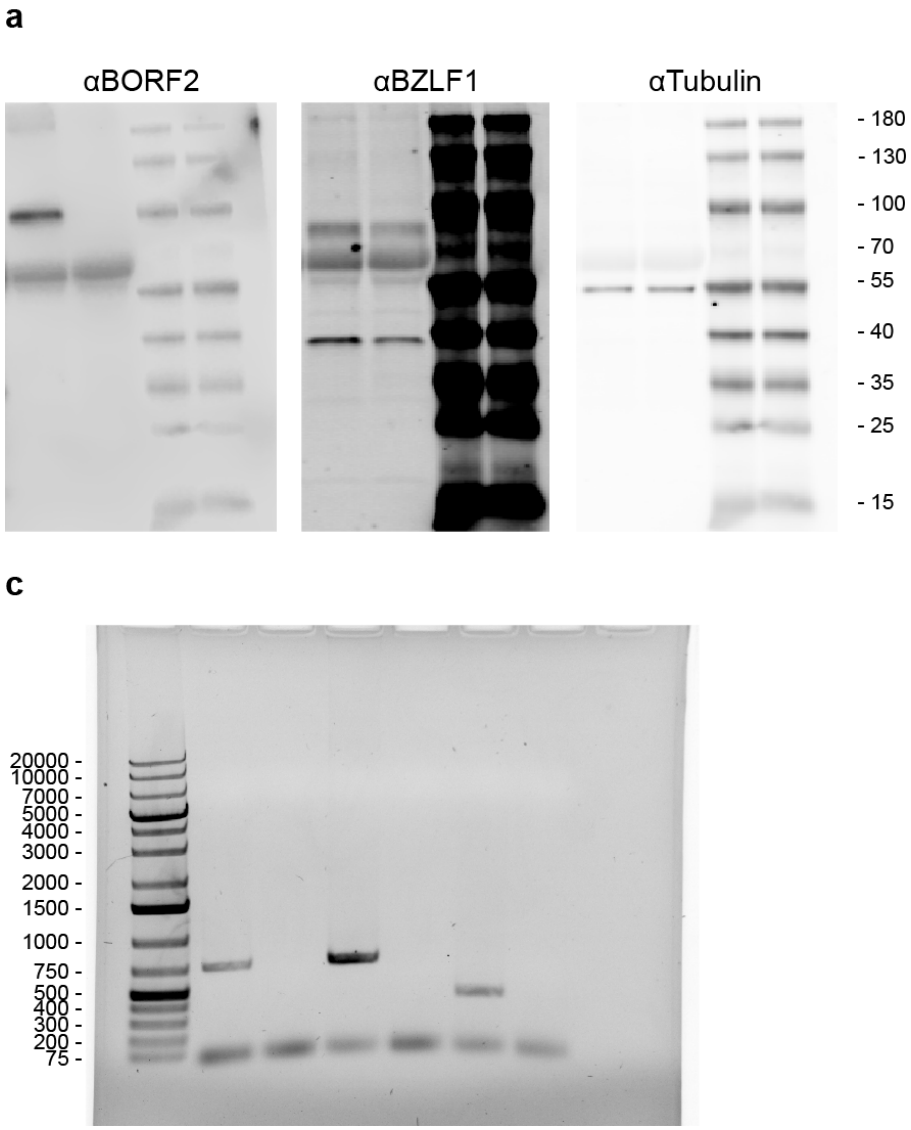

Legends for Supplementary Videos

Supplementary Video 1 | 3D-reconstruction of z-stacks show A3B/BORF2 aggregates colocalizing within endoplasmic reticulum.
Movie of 3D-reconstruction of z-stacks obtained in Fig. 4f through the entire cell depth, which shows U2OS cells transfected with A3B-mCherry, transduced with BORF2-eGFP, and stained with an antibody against the endoplasmic reticulum marker, BiP/GRP-78 (purple). z-stack images captured every 0.6 microns. These data are representative of n = 2 biologically independent experiments.

Supplementary Video 2 | z-series of reactivated AGS-EBV cells show BORF2 colocalization within endoplasmic reticulum.
Movie of z-series obtained from reactivated AGS-EBV cells through the entire cell depth, which shows cells stained with antibodies against BORF2 (red) and TRAPα (green). z-stack images captured every 0.3 microns. These data are representative of n = 2 biologically independent experiments.

Supplementary Video 3 | Live cell imaging showing effect of BORF2 induction on pre-existing A3B in U2OS cells.
Movie of U2OS cells which express A3B-mCherry at the time of initial data collection and immediately transduced with a lentivirus expressing BORF2-eGFP, which rapidly accumulates in protein levels as the movie progresses. These data are representative of n = 2 biologically independent experiments.

Supplementary Video 4 | Live cell imaging showing effect of BORF2 on A3B induction in U2OS cells.
Reciprocal movie of U2OS cells which express BORF2-eGFP, followed by induction of A3B-mCherry. These data are representative of n = 2 biologically independent experiments.